Structural Engineering and Mechanics, Vol. 22, No. 3 (2006) 311-330
DOI: http://dx.doi.org/10.12989/sem.2006.22.3.311

Post-peak response analysis of SFRC columns including spalling and buckling

Rajesh P. Dhakal†

Department of Civil Engineering, University of Canterbury, Private Bag 4800, Christchurch 8020, New Zealand

(Received May 17, 2005, Accepted October 21, 2005)

Abstract. Standard compression tests of steel fiber reinforced concrete (SFRC) cylinders are conducted to formulate compressive stress versus compressive strain relationship of SFRC. Axial pullout tests of SFRC specimens are also conducted to explore its tensile stress strain relationship. Cover concrete spalling and reinforcement buckling models developed originally for normal reinforced concrete are modified to extend their application to SFRC. Thus obtained monotonic material models of concrete and reinforcing bars in SFRC members are combined with unloading/reloading loops used in the cyclic models of concrete and reinforcing bars in normal reinforced concrete. The resulting path-dependent cyclic material models are then incorporated in a finite-element based fiber analysis program. The applicability of these models at member level is verified by simulating cyclic lateral loading tests of SFRC columns under constant axial compression. The analysis using the proposed SFRC models yield results that are much closer to the experimental results than the analytical results obtained using the normal reinforced concrete models are.

Key words: steel fiber reinforced concrete (SFRC); elasto-plastic and fracture (EPF) model; tension softening/stiffening model; cover spalling, reinforcement buckling; fiber analysis.

1. Introduction

Steel fiber reinforced concrete (SFRC) offers additional advantages over the normal reinforced concrete (RC). Some of these advantages can be enumerated as resistance against crack propagation, higher energy absorption, increased ductility, higher impact resistance, and better corrosion resistance. SFRC is also known for its enhanced shear capacity, which helps reduce the amount of shear reinforcement to render the construction easier. Because of the aforementioned advantages, SFRC columns under seismic loading are more likely to avoid shear failure and exhibit more ductile behavior than the normal RC columns. Even if designed to fail in flexure, normal RC columns exhibit spalling of cover concrete and buckling of reinforcing bars, which cause significant strength degradation in the post-peak large-displacement region. However in SFRC columns, these inelastic mechanisms are less likely to occur as the steel fibers maintain the integrity and provide additional confinement. Consequently, the post-peak flexural response of SFRC columns is expected to be more stable than that of normal RC columns.

† Senior Lecturer, E-mail: rajesh.dhakal@canterbury.ac.nz

There are several studies addressing the effect of steel fibers on the behavior of reinforced concrete (Fanella and Naaman 1982, Hsu and Hsu 1994, Someh and Saeki 1996) but none have led to cyclic material models for SFRC, without which the analytical research on the behavior of SFRC structures has not progressed much. The main objective of this study is to establish a tool to enable analytical study of members/structures made of SFRC. Hence, more emphasis is given to verify the ability rather than the accuracy of the established analytical tool. Standard compression tests of SFRC cylinders and pullout tension tests of SFRC specimens are conducted in order to obtain data to derive average stress-strain relationships of SFRC in compression and tension, respectively. Existing reinforcement buckling model (Dhakal and Maekawa 2002a,b) and cover concrete spalling model (Dhakal and Maekawa 2002c) are amended for SFRC and the spalling and buckling criteria are plugged in the constitutive equations of SFRC and reinforcing bars. In order to conduct cyclic analyses, the monotonic constitutive equations of SFRC and reinforcing bars are combined with corresponding unloading and reloading loops that are commonly used in cyclic models of normal RC (Okamura and Maekawa 1991). These nonlinear cyclic material models are then installed in a finite element analysis program which is used to perform fiber analyses of SFRC columns.

2. Compression model for SFRC

2.1 Compression tests

The range of volumetric fiber content used in SFRC is normally between 0 and 2.0%, and in most cases SFRC contains steel fibers close to 1% by volume. In this study, steel fiber content is hence adjusted to 1.0% by volume, which is believed to be the best representative value. Bridgestone steel fibers with hooked ends are used in the tests discussed here. These fibers are 40 mm in length, 0.5 mm in diameter, and have an aspect ratio of 80. Other constituent materials include cement (Ordinary Portland Cement with specific gravity 3.15), fine aggregate (sand with specific gravity 2.59, water absorption ratio 2.14 and uniformity coefficient 2.79) and coarse aggregate (gravel with specific gravity 2.66 and maximum size 20 mm). Altogether, 10 cylinders with 100 mm diameter and 200 mm height are prepared using the pre-specified materials so that the water to cement ratio (W/C) is equal to 0.5 and 0.6 for two sets of 5 specimens. The average slump of the mix is 50 mm for W/C = 0.5 and 54 mm for W/C = 0.6. All of these specimens are cured for 21 days; four specimens in air (dry curing) and six specimens in water (wet curing). These specimens are subjected to axial compression using a standard compression testing machine with a capacity of 1000 kN. To avoid friction, two layers of Teflon sheets sandwiched with silicon oil are used between the loading plate and the specimen. The compression loading rate is adjusted to 0.4~0.5 MPa/sec. Three parallel strain gauges are attached to each specimen and the average of these three gauge readings is used as the representative strain. The specimens are monotonically loaded in compression until the peak strain is reached, after which few unloading/reloading cycles are followed.

The compressive stress-strain curves obtained from the cylinder compression tests are shown in Fig. 1 and the compressive strength and the peak strain (i.e.; strain corresponding to the peak stress) are listed in Table 1. As in normal concrete, the compressive strength of SFRC cylinders with higher W/C ratio is less than that of the cylinders with lower W/C ratio. Moreover, the compressive strength of dry-cured specimens is slightly lower than that of wet-cured specimens. In both dry-

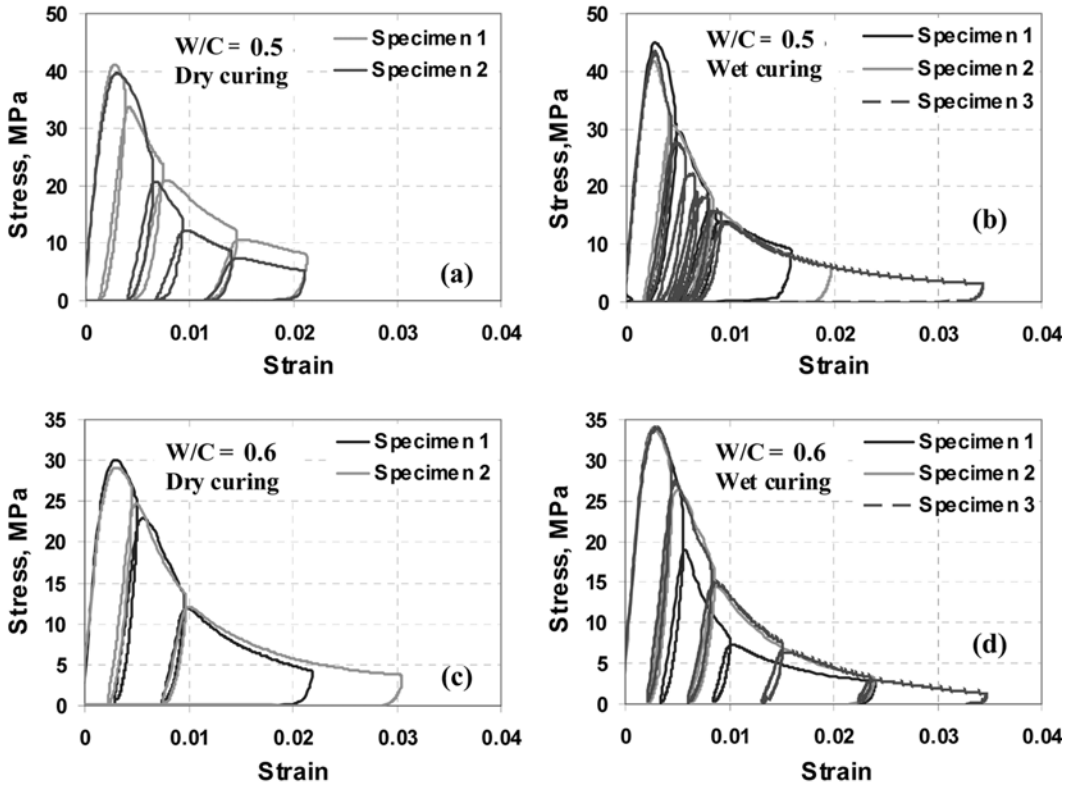

Fig. 1 Compressive stress-strain curves of SFRC cylinders

Table 1 Results of compression tests of SFRC cylinders

	W/C = 0.5		W/C = 0.6	
	Comp. Strength (MPa)	Peak strain ($\mu\varepsilon$)	Comp. Strength (MPa)	Peak strain ($\mu\varepsilon$)
Dry curing	41.1	2743	30.1	2984
	39.6	2961	29.1	3183
Wet curing	44.7	2840	33.9	3008
	41.7	2628	34.0	2846
	43.2	2729	34.0	2827

cured specimens, the peak strain of specimens with higher W/C ratio is higher than that of specimens with lower W/C ratio. Similar trend is found in wet-cured specimens, although one wet-cured specimen with W/C = 0.6 has a peak strain of 2827 $\mu\varepsilon$ which is just below the highest peak strain (i.e., 2840 $\mu\varepsilon$) observed in the three wet-cured specimens with W/C = 0.5.

2.2 EPF model for normal concrete

For normal concrete, elasto-plastic and fracture (EPF) model (Maekawa and Okamura 1983) can

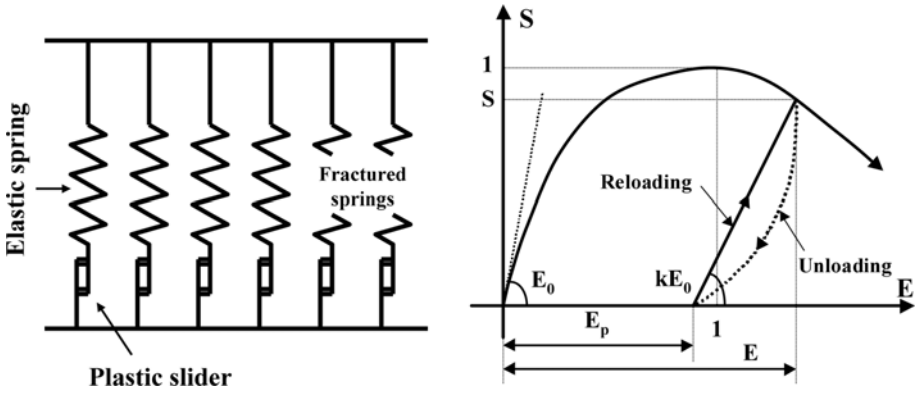

Fig. 2 Elasto-plastic and fracture (EPF) model (Maekawa and Okamura 1983)

accurately trace the stress-strain relationship during monotonic compression loading as well as unloading from and reloading to compression. The basic concept of this model is illustrated in Fig. 2. Concrete is modeled as a combination of some constituent elements parallel to each other. Each element consists of an elastic spring and a plastic slider in a series. The plastic components represent the plasticity related to the degree of accumulated damage and the number of broken elastic springs represents the compressive fracture leading to a reduction of the unloading/reloading stiffness. The overall nonlinearity of concrete in compression is represented by two parameters, namely equivalent plastic strain E_p and the fracture/damage parameter K. Plastic strain is defined as the strain remaining when the stress is unloaded to zero and the fracture parameter is defined as the ratio of unloading/reloading stiffness to the initial stiffness. Both of these parameters depend on the maximum compressive strain experienced by the concrete.

In Fig. 2, the relationship between equivalent compressive stress and equivalent compressive strain is also shown. For uniaxial loading, equivalent stress and equivalent strain are the absolute stress and absolute strain normalized with respect to the compressive strength and the peak strain, respectively. According to the EPF model, the relationship between the equivalent compressive stress S and the equivalent compressive strain E is given by Eq. (1).

$$S = E_0 K(E - E_p) \tag{1}$$

In Eq. (1), E_0 is the equivalent initial elastic stiffness of concrete and its value is equal to 2. The fracture parameter K and the equivalent plastic strain E_p for normal concrete are expressed as given in Eq. (2) and Eq. (3) respectively. In Eq. (3), C is a constant that depends on the loading rate. For normal loading rate, its value is experimentally determined to be equal to 20/7.

$$K = \exp[-0.73E(1 - \exp(-1.25E))] \tag{2}$$

$$E_p = E - C[1 - \exp(-0.35E)] \tag{3}$$

It is known that the addition of steel fibers affects the peak strain and, to a lesser extent, the compressive strength (Kosaka *et al.* 1984, Someh and Saeki 1996). It is therefore meaningless to compare the absolute values of stresses and strains in normal concrete and SFRC. Alternately, the

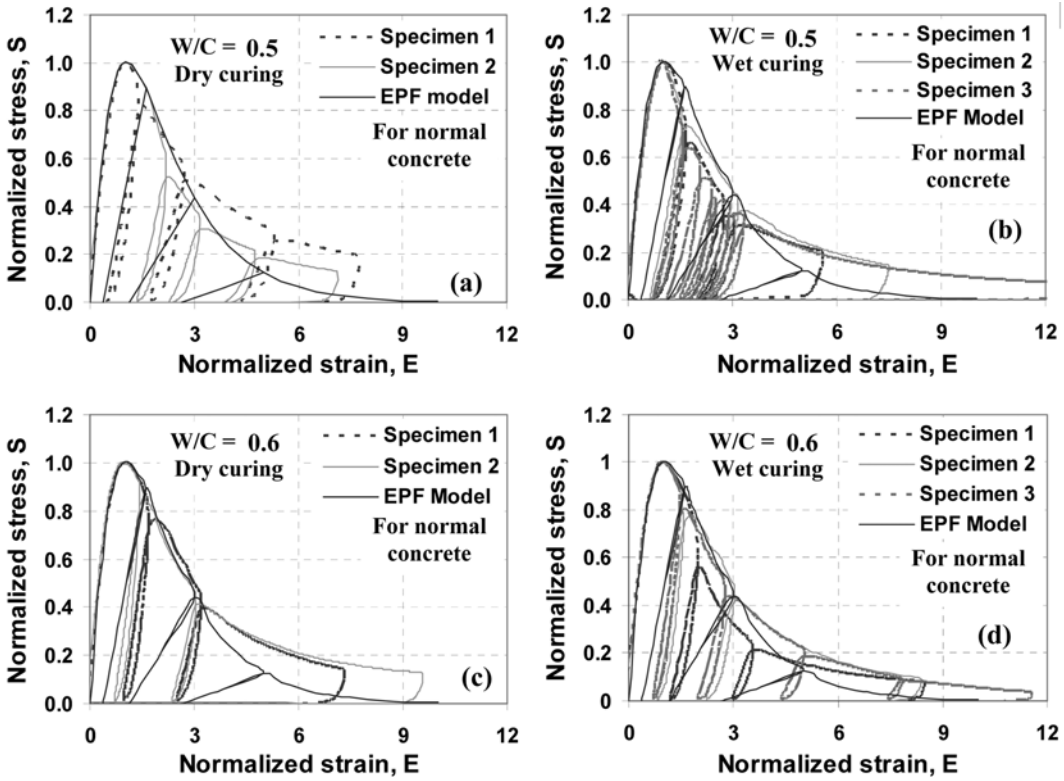

Fig. 3 Equivalent stress-strain curves for SFRC and comparison with the EPF model for normal concrete

stresses and strains should be normalized with respect to the peak stress and peak strain respectively and the normalized stress-strain plots should be compared to reach more rational conclusions as such curves are independent of the peak stress and the peak strain. It may also be possible to represent such normalized stress-strain plots by Eq. (1) of the EPF model. In Fig. 3, the stress-strain curves obtained from the compression tests of SFRC cylinders are normalized with respect to the compressive strength and the peak strain. In addition, similar curves produced for normal concrete using Eqs. (1)-(3) are also plotted in Fig. 3.

It can be observed from the plots that the EPF model for normal concrete can closely trace the equivalent stress-strain behavior of SFRC in the pre-peak region. However, compressive stress in the post-peak high strain range predicted by the EPF model for normal concrete is less than that obtained from the SFRC cylinder tests. In addition, the unloading behavior predicted by the EPF model for normal concrete is also different from that obtained from the compression tests of SFRC cylinders, which exhibits significantly higher unloading/reloading stiffness.

2.3 Modified EPF model for SFRC

From the test data, the equivalent plastic strain E_p and the fracture parameter K for different level of equivalent compressive strain are extracted. As the cylinders were subjected to a few cyclic strain reversals in the post-peak range, the plotted equivalent stress-strain curves also include unloading

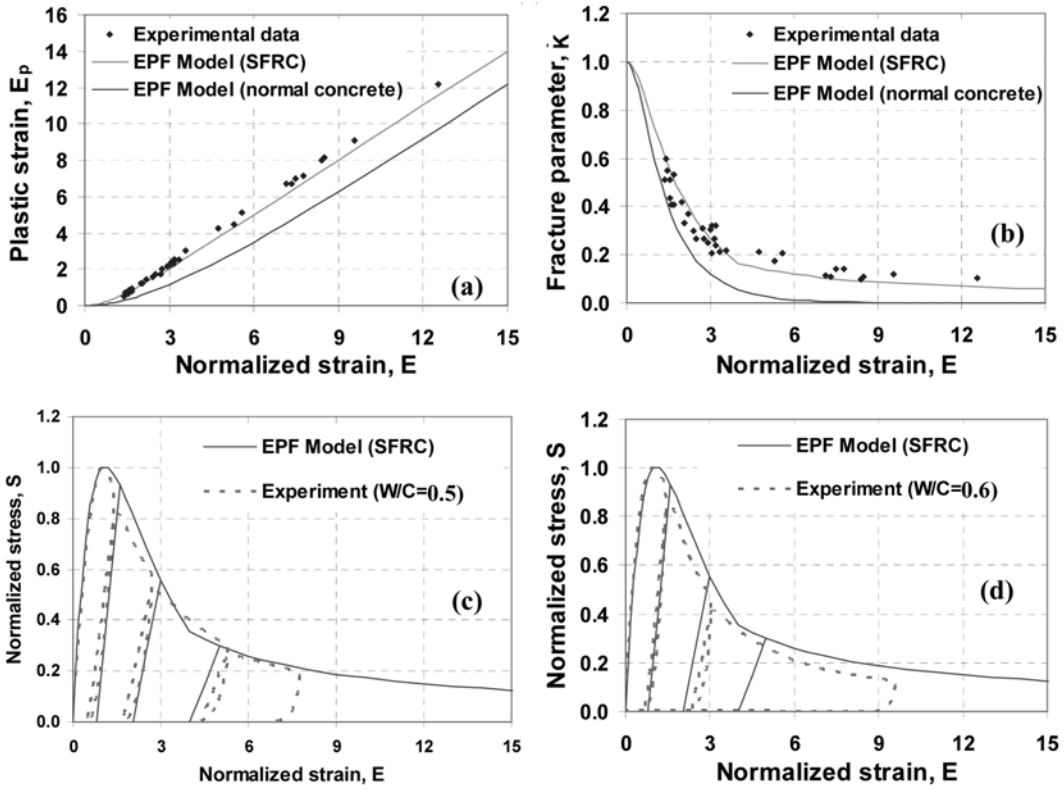

Fig. 4 Modified EPF model and comparison with experimental curves

and reloading paths. Otherwise, it would not be possible to obtain E_p (equivalent strain remaining at zero stress after unloading) and K (normalized average unloading/reloading stiffness). In Figs. 4(a) and (b), the values of E_p and K obtained from the test results are compared with the corresponding parameters calculated using Eqs. (2) and (3) of the original EPF model. The comparison reveals that the equivalent plastic strain and the fracture parameter of SFRC are different from those of normal concrete, especially in the high strain range. The equivalent plastic strain obtained from the SFRC cylinder tests is slightly higher than that predicted by the original EPF model whereas the fracture parameter of SFRC is significantly higher than that predicted by the EPF model for normal concrete. The increase in the values of these parameters is attributable to the presence of steel fibers, which help maintain the toughness even after the mechanical fractures such as cracking and crushing occur.

As Eq. (1) suggests, if the fracture parameter K is constant, an increase in the plastic strain reduces the post-peak compressive stress. In contrast, an increase in the fracture parameter keeping the plastic strain constant results in a higher post-peak compressive stress. Hence, the combination of a small increase in plastic strain and a larger increase in fracture parameter obviously causes an increase in the post-peak compressive stress. To correlate better with the test results, modified equations for the equivalent plastic strain E_p and the fracture parameter K are proposed for SFRC:

$$E_p = E - [1 - \exp(-E)] \tag{4}$$

$$K = \exp[-0.45E(1-\exp(-1.25E))] \quad \text{for} \quad E \le 4$$
$$K = 0.5E^{-0.8} \quad \text{for} \quad E > 4 \tag{5}$$

Using these two modified equations for E_p and K, equivalent stress can now be calculated using Eq. (1). Note that Eq. (1) does not need to be changed and can be readily applied for SFRC, but with the modified values of E_p and K. Moreover, the initial equivalent stiffness E_0 is found to be equal to 2.18 from the test results. The comparative curves produced by Eqs. (1), (4) and (5) are plotted with the test results in Fig. 4(c) and Fig. 4(d). The comparison between these modified equations and the test results shows that the proposed model could accurately predict the compressive stress even in the post-peak high-strain range and the unloading and reloading paths could also be fairly captured. The increased post-peak compressive stress is also predicted by the proposed model. Note that the aforementioned equations are derived from the test results of SFRC cylinders with 1% fiber content and may not accurately represent the behavior of SFRC with different fiber content. When the fiber content decreases, the peak strain and the post-peak compression softening of SFRC become closer to those of normal concrete (Someh and Saeki 1996), and the fracture parameter and plastic strain should be changed accordingly to reflect this.

3. Spatially averaged tension model for SFRC

3.1 Tension softening/stiffening model for normal concrete

Axial tension causes discrete tensile cracks in reinforced concrete, and at the cracked section concrete does not carry any normal stress. However, in between these cracks, concrete still carries some tensile stress due to bond between the reinforcing bars and concrete. Hence, the average post-cracking tensile stress carried by concrete between the cracks is not zero. According to the tension softening/stiffening model illustrated in Fig. 5, the average tensile stress-strain relationship of cracked concrete is expressed as shown in Eq. (6) (Okamura and Maekawa 1991).

$$\sigma = f_t\left(\frac{\varepsilon_{cr}}{\varepsilon}\right)^c \tag{6}$$

Here, f_t is the tensile strength of normal concrete and ε_{cr} is the cracking strain, assumed as two times the elastic strain at tensile strength. Similarly, c is the tension stress release parameter that

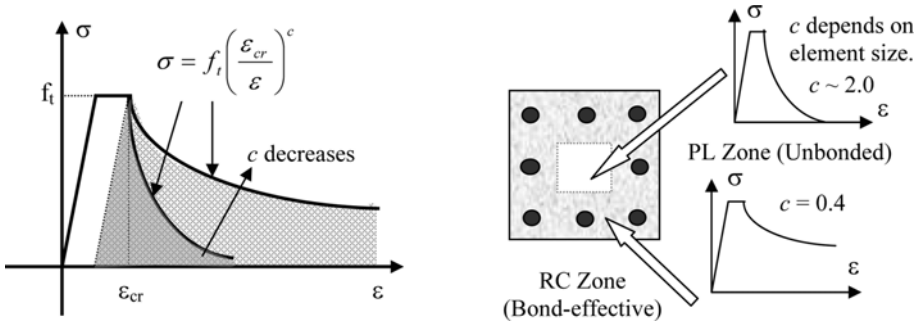

Fig. 5 Tensile stress-strain relationship of cracked concrete

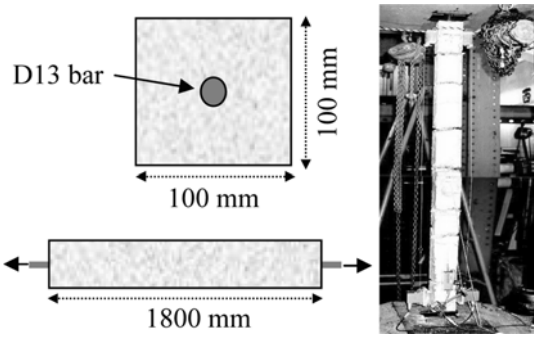

Fig. 6 Specimen and setup for pullout test

solely defines the post-cracking response. This parameter accounts for the bond between the concrete and surrounding reinforcing bars, and hence depends on the amount of reinforcement. For normal concrete with substantial reinforcement, c takes a smaller value resulting in a higher post-cracking stress in concrete, and vice versa. For assigning representative values of c, RC zoning method (An *et al.* 1997) is used; i.e., concrete is divided into two zones according to its distance from the nearest reinforcing bar (see Fig. 5). Concrete far from reinforcement is defined as the PL (plain concrete) zone and the RC (reinforced concrete) zone consists of the concrete within the bond-effective region. In case of normal concrete without steel fibers, the value of tension stress release parameter c takes a value of 0.4 for the RC zone and approximately 2 for the PL zone. Using these values of c, Eq. (6) automatically switches to tension-stiffening model for reinforced concrete and tension-softening model for plain concrete.

3.2 Pullout tests and results

In order to establish the tensile stress-strain relationship of SFRC, axial pullout tests of SFRC specimens are performed. Two test beams, one each with water cement ratio 0.5 and 0.6 are prepared. As shown in Fig. 6, the specimen is of 100 mm square cross-section and its length is 1800 mm. A reinforcing bar of 13 mm diameter is included in the middle of the cross-section. Using a standard tension test device, axial tension is applied to the reinforcing bar and the average strain in the beam is measured. The relationships between the applied load and the average strain for the two specimens are shown in Figs. 7(a) and (b), respectively.

The tensile load versus strain relationship of the reinforcing bar is established through a separate axial tension test of the D13 steel bar. The elastic modulus and yield strength of the reinforcing bar are found to be 189 GPa and 329 MPa, respectively. The bare bar stress-strain curve is then modified to account for the effect of bond between concrete and reinforcing steel. As the bond behavior between SFRC and reinforcing bars is not quantified, the average stress-strain relationship of reinforcing bars is derived by using a similar method commonly used for normal RC (Okamura and Maekawa 1991). The modified average load versus strain curve for the reinforcing bar is also shown in Figs. 7(a) and (b). The average load carried by the reinforcing bar is then deducted from the total load carried by the SFRC beam to obtain the contribution of the cracked SFRC. As expected, the test results show that SFRC carries significant tension in the post-cracking high-strain range.

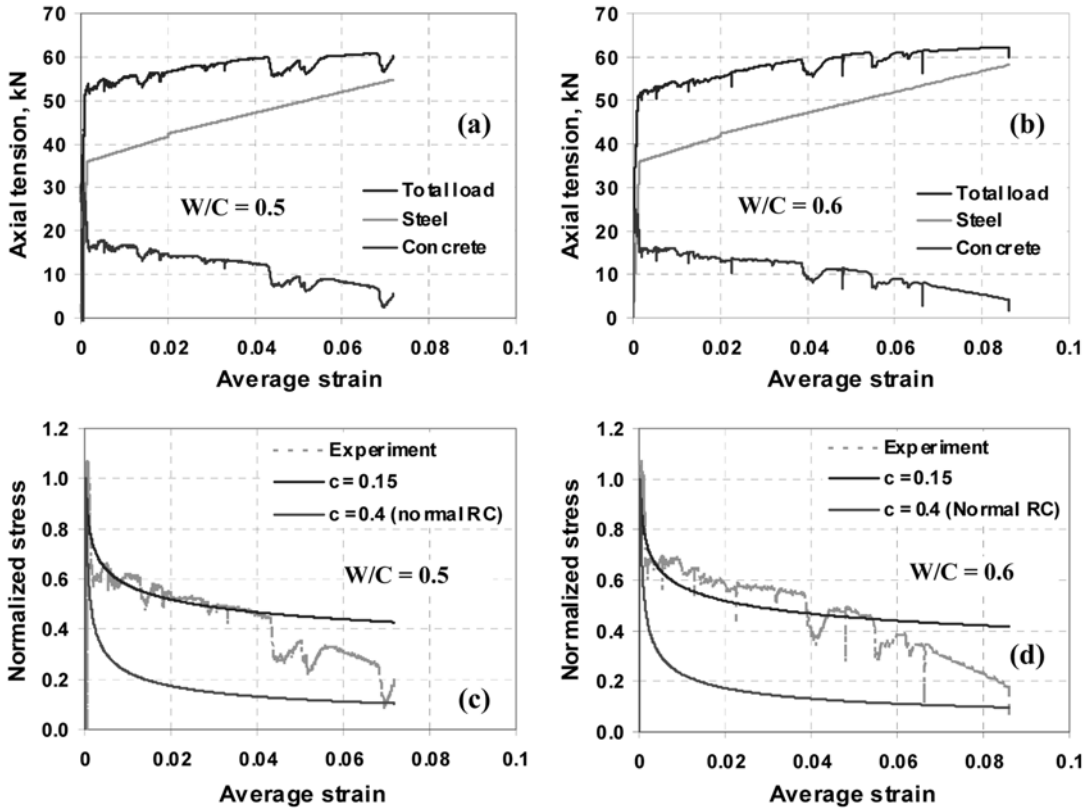

Fig. 7 Pullout test results and modeling of tensile behavior of SFRC

3.3 Modified tension model for SFRC

In order to determine the value of tension stress release parameter c for SFRC, Eq. (6) is calibrated against the tensile stress-strain curve of SFRC. First, the load carried by the cracked SFRC is divided by the cross section area to obtain the tensile stress, which is then normalized with respect to its maximum value (i.e.; tensile strength of SFRC). The normalized average tensile stress versus absolute strain curves are plotted in Figs. 7(c) and (d). These plots also include similar curves predicted by using two different values of tensile stress release parameter in Eq. (6); (i) c = 0.4 as in normal RC, and (ii) c = 1.5 proposed for SFRC. The tensile stress-strain curves plotted from the test data in both cases are close to the curves predicted using c = 0.15. As the SFRC in the cross-section is in the bond-effective RC zone, c = 0.15 is hence assigned for the RC zone inside SFRC members. Note that this value of c is derived from the test results with 1% fiber content and it may change depending on the amount of fibers. If the fiber content is 0%; i.e., normal concrete, c must equal 0.4. Furthermore, if the fiber content increases, the post-cracking tensile stress also increases and the value of c must decrease to reflect this. The value of c for the unbonded PL zone in SFRC with 0% steel fibers (i.e., normal concrete) is obviously equal to 2, and for a high fiber content, the bond between concrete and steel fibers render SFRC equivalent to the bond-effective zone of normal concrete and the value of c must be close to 0.4. As the relationship between the

fiber content V_f and tension stress release factor c has not yet been established, it is assumed that c for unreinforced SFRC with 1% fibers is 0.4; i.e., the same as that for the RC zone of normal concrete. Hence, c equal to 0.15 (RC zone) and 0.4 (PL zone) is used in the forthcoming fiber analysis of SFRC columns.

4. Reinforcement buckling and cover spalling in SFRC

4.1 Cyclic stress-strain relationships of reinforcing bars including buckling

Cyclic stress-strain relationships of reinforcing bars have been established, verified and incorporated into a finite-element based fiber analysis tool (Dhakal and Maekawa 2002b). These constitutive equations are fully path-dependent and take into account the effect of buckling of reinforcing bars in compression. The compressive stress carried by a bar decreases due to buckling. The average compressive stress versus average compressive strain relationship of a bare bar is schematically illustrated in Fig. 8 (Dhakal and Maekawa 2002a). As can be seen in the figure, the average compressive stress for a given strain is less than the local/tensile stress corresponding to the same strain. The average compressive stress-strain curve is linear until yielding, after which the ratio of the average compressive stress to the tensile/local stress decreases linearly until a pre-determined intermediate point. After this point the average compression envelope follows a linear softening path with a softening modulus of $0.02E_s$ (2% of the Young's modulus) until a strain where the average stress equals $0.2f_y$ (20% of the yield strength), beyond which the average compressive stress is kept constant at $0.2f_y$. Note that the compression envelope is completely described by the coordinates (ε_i, σ_i) of the intermediate point, which depend solely on the *buckling parameter* λ_b. The *buckling parameter* is defined as the product of slenderness ratio and the square root of the yield strength; i.e., $\lambda_b = L/d_b \times \sqrt{f_y}$, where L is the buckling length and d_b is the diameter of the compressed bar. Cyclic stress-strain relationship of a bare-bar is obtained by combining this monotonic compression envelope with the standard tension envelope and unloading/reloading loops described by the Giuffre-Menegotto-Pinto model (CEB 1996).

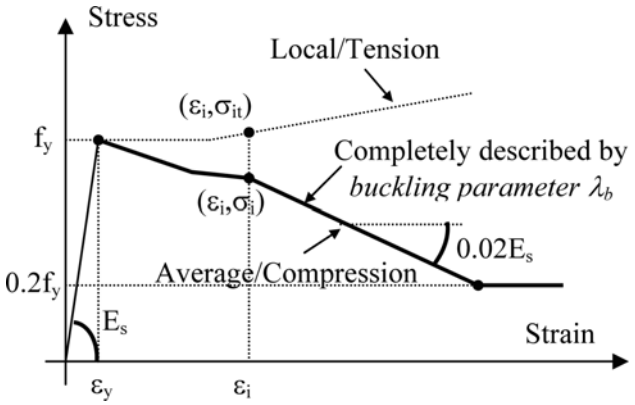

Fig. 8 Bare-bar buckling model (Dhakal and Maekawa 2002a)

Table 2 Required lateral stiffness for different buckling modes (Dhakal and Maekawa 2002c)

Mode, n	1	2	3	4	5	6	7	8
κ_{eq}	0.7500	0.1649	0.0976	0.0448	0.0084	0.0063	0.0037	0.0031

4.2 Buckling length of reinforcing bars in SFRC

As the diameter d_b and the yield strength f_y of a bar are its inherent properties and cannot be changed, the only constituent of the *buckling parameter* λ_b that affects the average compressive stress-strain relationship of a given bar is L; i.e., the buckling length. Hence, an accurate and reliable method to predict the buckling length of main bars is needed to complement the aforementioned constitutive model. The buckling of main bars inside normal RC members may be restricted within two consecutive ties or may span several tie-spacing depending on the geometrical and mechanical properties of the main bars and the lateral ties (Dhakal and Maekawa 2002c). In reinforced SFRC members, the quantity of steel fibers also contribute in reducing the potential buckling length of the main bars. An existing method to determine the buckling length of main bars inside normal RC members (Dhakal and Maekawa 2002c) will be modified in this study to extend its application to SFRC.

In this method, the effective anti-buckling stiffness of a system of lateral ties is calculated as shown in Eq. (7), where n_l is the number of tie-legs along the buckling direction and n_b is the number of main bars lying in the extreme layer that are likely to buckle simultaneously. In Eq. (7), E_t, A_t and l_t are respectively the elastic modulus, cross-sectional area and the effective length of the ties' side-legs that are pulled in tension when the compressed main bars buckle.

$$K_t = \frac{E_t A_t}{l_t} \times \frac{n_l}{n_b} \tag{7}$$

Similarly, the lateral stiffness at the position of the ties required to hold the compressed main bars in various buckling modes (ratio of the buckling length L to the tie-spacing s) is derived based on energy principle taking into account the interaction between the lateral ties and main bars. The normalized dimensionless values of the required lateral stiffness K_{eq} for the first eight buckling modes are shown in Table 2 (Dhakal and Maekawa 2002c). The absolute value of the required lateral stiffness corresponding to a buckling mode is to be calculated as shown in Eq. (8), where EI is the compressed main bar's average flexural rigidity estimated as suggested in Eq. (8), E_s is the Young's modulus, and I is the moment of inertia of the main bar.

$$K_n = K_{eq} \times \frac{\pi^4 EI}{s^3} \qquad EI = \frac{E_s I}{2}\sqrt{\frac{f_y}{400}} \tag{8}$$

Comparing the effective anti-buckling tie stiffness K_t with the required lateral stiffness K_n, the stable buckling mode can be determined, which is the lowest mode for which K_n is less than K_t. Buckling length is then calculated by multiplying the buckling mode with the tie-spacing. The same method can be used to determine the buckling length of main bars in SFRC members with lateral ties, but the additional anti-buckling stiffness provided by the still fibers should be added to the tie stiffness K_t before comparing with the required stiffness K_n. In order to quantify the anti-buckling stiffness of the steel fibers, the continuum of steel fibers is replaced by discrete elastic springs at the two extremes of the buckling length (see Fig. 9). As shown in Fig. 9, one discrete spring acting

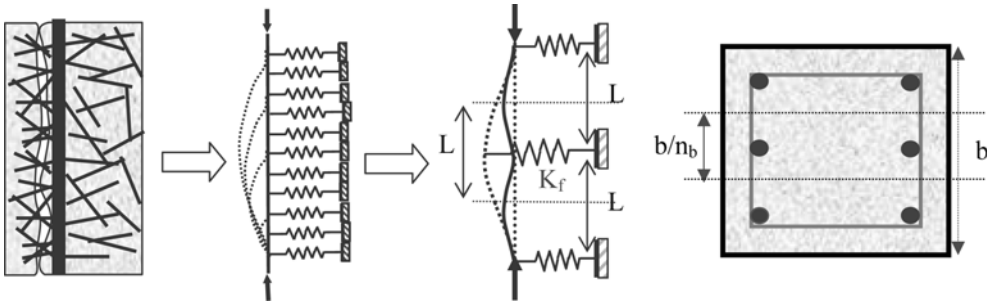

Fig. 9 Determination of buckling length in SFRC

against the buckling of one main bar represents the steel fibers inside an area ($L \times b/n_b$), where L is the buckling length, b is the section width, and n_b is the number of main bars in the extreme layer. As this buckling configuration corresponds to the first buckling mode, the value of the required equivalent stiffness can be borrowed from Table 2 (i.e., $K_{eq} = 0.75$). Hence, if the contribution of the ties is not taken (or if the ties are not provided), the steel fibers must provide a lateral stiffness K_{freq} to be calculated as in Eq. (9).

$$K_{freq} = \frac{3\pi^4 EI}{4L^3} \tag{9}$$

The amount of steel fibers in SFRC is quantified by its volumetric ratio V_f. The fibers are randomly aligned along all possible directions in a three-dimensional space, but the anti-buckling stiffness is contributed only by the axial stiffness of fibers aligned along the buckling direction or the component of other fibers' stiffness along the buckling direction. Assuming homogeneous distribution and orientation of fibers, equivalent volumetric fraction of fibers aligned in one specific direction is equal to $V_f/3$ and the corresponding area ratio perpendicular to any plane becomes $(V_f/3)^{2/3}$. The equivalent area of steel fibers represented by a spring is hence equal to $(Lb/n_b) \times (V_f/3)^{2/3}$. If the length and elastic modulus of the fibers are denoted respectively by l_f and E_f, the axial stiffness of one representative spring can be calculated as in Eq. (10).

$$K_f = \frac{E_f}{l_f} L \frac{b}{n_b} \left(\frac{V_f}{3}\right)^{2/3} \tag{10}$$

Comparing Eq. (9) and Eq. (10), the buckling length L can be calculated as

$$L = 3.51 \times \left(\frac{EI \times l_f \times n_b}{E_f \times b \times V_f^{2/3}}\right)^{1/4} \tag{11}$$

The buckling length calculated by Eq. (11) can be applied without any modification to SFRC members without lateral ties. If lateral ties are provided, the calculated buckling length L should be compared with the tie-spacing s. In some cases L might turn out to be less than s, which means that the ties are not activated and the buckling length is controlled by the steel fibers only. On the other hand, if the tie-spacing s is less than the buckling length L calculated by Eq. (11), the lateral ties will be pulled when the main bars buckle and the tie stiffness must be included before deciding the buckling length. The anti-buckling stiffness of such SFRC members K_{SFRC} is contributed by the lateral ties and the steel fibers and can be calculated as

$$K_{SFRC} = K_t + K_f = \frac{E_t A_t}{l_t} \times \frac{n_l}{n_b} + \frac{E_f}{l_f} L \frac{b}{n_b} \left(\frac{V_f}{3}\right)^{2/3} \tag{12}$$

In order to determine the stable buckling mode and the corresponding buckling length of main bars in SFRC members, the total anti-buckling stiffness K_{SFRC} calculated from Eq. (12) should be compared with the required lateral stiffness K_n calculated from Eq. (8) and Table 2. Note that L in the right hand side of Eq. (12) is to be substituted by the product of the tie-spacing s and the buckling mode being checked against. Thus determined value of the buckling length can be used to generate the average compressive stress-strain relationship of main bars to be used in the fiber analysis of SFRC structures. As expected, if the fiber content is zero Eq. (12) proposed for SFRC coincides with Eq. (7) aimed for normal RC, indicating that this method may be applicable for any combination fiber content and lateral ties.

4.3 Spalling of cover concrete in SFRC

When RC members are subjected to flexure, the cover concrete in the compression side of plastic hinges disintegrates and looses further load-carrying capacity; a phenomenon known as spalling. In SFRC members, although splitting cracks may be formed, cover spalling is delayed due to the presence of fibers which bridge these cracks and maintain the integrity. For analytical modeling, it is important to know when the cover concrete spalls so that the compressive stress otherwise assigned to the cover concrete fibers by the EPF model could be adjusted to zero. The compressive strain of main bars required to cause spalling of adjacent cover concrete in normal RC members has been quantified (Dhakal and Maekawa 2002c). In this study, the same method is extended to predict the spalling strain in SFRC members.

For complete cover spalling, wide splitting cracks unable to carry normal stress must be formed between the cover concrete and core concrete; i.e., next to the compression bars. The splitting cracks initiate due to the axial compressive strain in the cover concrete and these cracks are further widened by the lateral deformation of the compressed main bars. After subtracting the equivalent crack width due to the axial compression from the crack width corresponding to zero tensile stress, the lateral deformation of the compressed bars and the corresponding average compressive strain required to completely spall the surrounding cover concrete is calculated. According to the spalling model (Dhakal and Maekawa 2002c), the plastic compressive strain ε_p^{sp} in the main bars required to cause complete spalling of surrounding cover concrete can be estimated as

$$\varepsilon_p^{sp} = \frac{\pi^2}{4L^2} \times \left(\frac{(4+K) \times G_F}{f_t}\right)^2 \tag{13}$$

In Eq. (13), K, f_t and G_F are the fracture parameter, tensile strength and the fracture energy of the concrete, respectively. The total compressive strain in the main bars corresponding to the complete spalling of surrounding cover concrete is obtained as the sum of the elastic component; i.e., the yield strain, and the plastic strain ε_p^{sp} calculated from Eq. (13). Once the compressive strain in nearby main bars equals this value, the compressive stress carried by cover concrete is reduced to zero. In this study, Eq. (13) is applied without any modification to establish the spalling criteria in SFRC members. However, the values of the parameters in the right hand side of this equation must correspond to those of SFRC.

The fracture parameter K for SFRC should be calculated using Eq. (5), and the buckling length L

should be determined as explained in the previous chapter. Obviously, the value of K is slightly higher and that of L is either equal to or smaller in SFRC than in normal concrete. The tensile strength f_t of normal concrete can be used for SFRC as the presence of fibers improves the post-cracking tensile performance but is believed to have little influence on the tensile strength itself (Matsuoka *et al.* 1997). The other parameter in Eq. (13) is the fracture energy G_F, which differs the most between normal concrete and SFRC and hence influences the final outcome more than the others do. Fracture energy G_F is defined as the energy required to form a crack of unit area that cannot transfer tensile stress anymore, and its value is believed to be larger for SFRC than for normal concrete owing to the bridging action of the steel fibers. It is experimentally found that the fracture energy of SFRC ranges between 0.6-5 N/mm depending on the fiber content (Matsuoka *et al.* 1997), which is much higher than that of normal concrete (around 0.1 N/mm). This drastic increase in the value of G_F combined with a larger K and smaller L will lead to a substantially high value of the plastic spalling strain ε_p^{sp} in SFRC members than in RC members, rightly predicting that the cover spalling is significantly delayed in SFRC.

4.4 Effect of fiber content on spalling and buckling in SFRC

For qualitative verification of the proposed spalling and buckling models, the effect of fiber content on the buckling length and the resulting spalling strain and average compressive stress-strain relationship of reinforcing bars is investigated. As shown in Fig. 10, a 200 mm square column

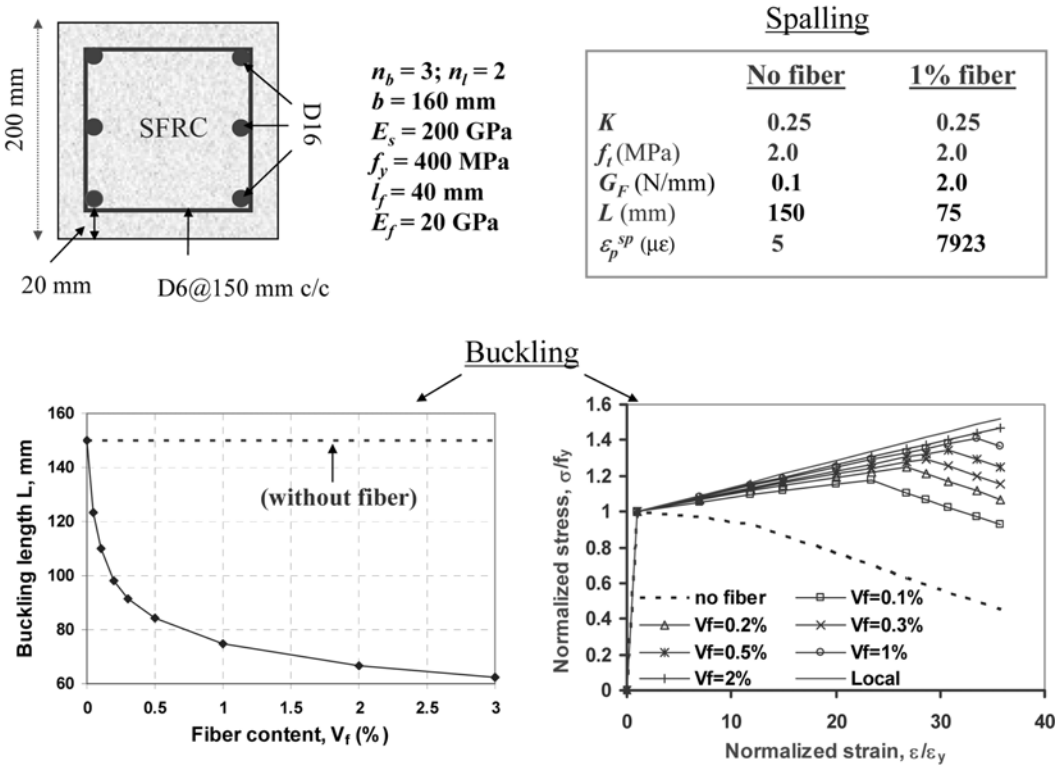

Fig. 10 Effect of fiber content on spalling and buckling in SFRC members

reinforced with three 16 mm diameter bars in each side and 6 mm diameter two-legged ties spaced at 150 mm is adopted. The volumetric ratio of steel fibers is varied from 0% to 2%, and the length l_f and modulus E_f of the fibers are assumed to be 40 mm and 200 GPa, respectively. Note that the objective is to see if the interrelationship between the fiber content and the spalling/buckling mechanisms in the proposed models is sensible, and the member on which the parametric study is performed need not satisfy any design guidelines. Hence, the geometrical and mechanical properties of the cross-section are chosen arbitrarily.

The variation of buckling length with respect to the fiber content and the corresponding average compressive stress-strain curves are also plotted in Fig. 10. If no fibers are used, the main bars buckle in the first mode; i.e., $L = s = 150$ mm. When the steel fibers are added, the buckling length L calculated using Eq. (11) turns out to be smaller than the tie-spacing. The buckling length is found to decrease exponentially with an increase in fiber content. Consequently, as the fiber content increases the effect of reinforcement buckling in the compression response gradually diminishes and the average compressive stress-strain envelope moves closer to the tension envelope. These findings qualitatively agree with the experimental fact that the reinforcement buckling in SFRC flexural columns is significantly retarded compared to that in normal RC columns (Masuda *et al.* 1997).

In order to calculate the spalling strain, the following values are assumed: $K = 0.25$; $f_t = 2$ MPa. The values of fracture energy G_F of concrete without steel fibers and with 1% steel fiber are fairly assumed to be equal to 0.1 N/mm and 2.0 N/mm, respectively (Matsuoka *et al.* 1997). With no steel fiber, the buckling length is equal to the tie-spacing, i.e., 150 mm. The corresponding plastic spalling strain ε_p^{sp} calculated by Eq. (13) is 5 $\mu\varepsilon$, indicating that cover spalling takes place just after the main bars are subjected to yielding strain in compression. However, for SFRC with 1% fiber content, the buckling length calculated using Eq. (11) is approximately equal to 75 mm. This reduced value of L combined with a significantly large fracture energy G_F leads to a very high value of the plastic spalling strain ε_p^{sp} (7923 $\mu\varepsilon$). Thus, the delay of cover spalling in SFRC can be captured by Eq. (13).

5. Application of proposed models

5.1 Finite-element based fiber analysis

Next, fiber analyses using a finite-element analysis tool COM3 (*Co*ncrete *M*odel in *3*D) (Maekawa 2000) are performed to predict cyclic behavior of SFRC columns. In COM3, beams and columns are represented by frame elements, which are analyzed by fiber technique (Menegotto and Pinto 1973). In fiber technique, each element is represented using a single line and the member cross-section is divided into many cells or sub-elements. The strain of each cell is calculated based on the Euler-Kirchoff's hypothesis, i.e., plane section remains plane after bending. For each fiber strain along the axis of finite element, stress is calculated using the material constitutive models (i.e., stress-strain relationships) representing the average behavior in the finite-element domain. The proposed monotonic envelopes for SFRC and reinforcing bars are summarized in Fig. 11. The tension and compression envelopes of reinforcing bars are combined with unloading/reloading rules (Dhakal and Maekawa 2002b) to form a path-dependent cyclic model. As reliable cyclic models for SFRC are not yet available the path-dependent unloading and reloading loops used for normal concrete (Okamura and Maekawa 1991) are combined with the SFRC monotonic envelopes to form a cyclic model.

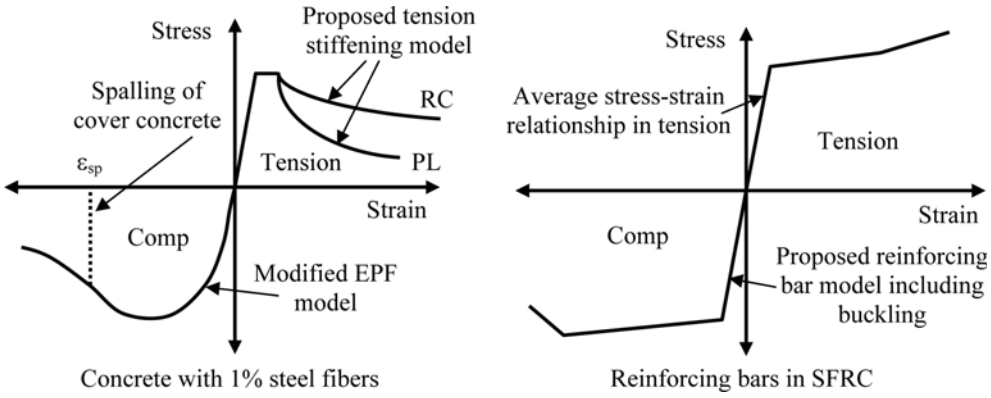

Fig. 11 Constitutive models for fiber analysis of SFRC members

In fiber technique, the stress field is reduced to one dimension along the axis of finite element or members. The shear force is computed so that it is in equilibrium with the flexural moment field. The in-plane shear deformation is considered based on Timoshenko's beam theory, i.e., linear in-plane shear behavior is assumed. As inelastic shear deformation is ignored, shear failure will not be captured. Conclusively, this fiber analysis tool is suitable for structures whose shear strength is high enough to ensure that flexural failure occurs before the shear response enters the inelastic range.

5.2 Cyclic behavior of SFRC columns

The experimental results of Masuda *et al.* (1997) are adopted for assessing the applicability of the proposed models and the established tool. These experiments were conducted to study the failure modes of SFRC columns. It was found that the presence of steel fibers enhances the shear performance. Most of the tested SFRC columns failed in flexure although the calculated shear capacity for similar normal RC columns was considerably smaller than their flexural capacity, and similar columns without steel fibers failed in shear. Two columns, the responses of which were least affected by shear deformation, are chosen for comparison with analytical results. The details of the test specimens are shown in Fig. 12. As shown in the figure, both SFRC columns have 1% steel

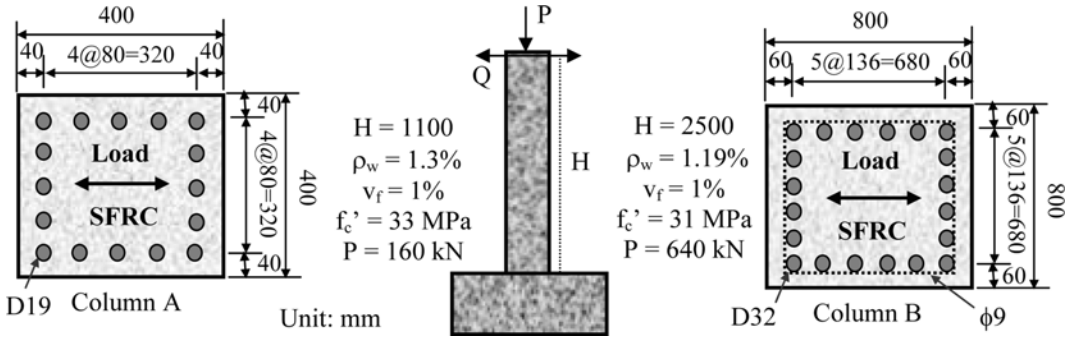

Fig. 12 Specimen details and experimental setup (Masuda *et al.* 1997)

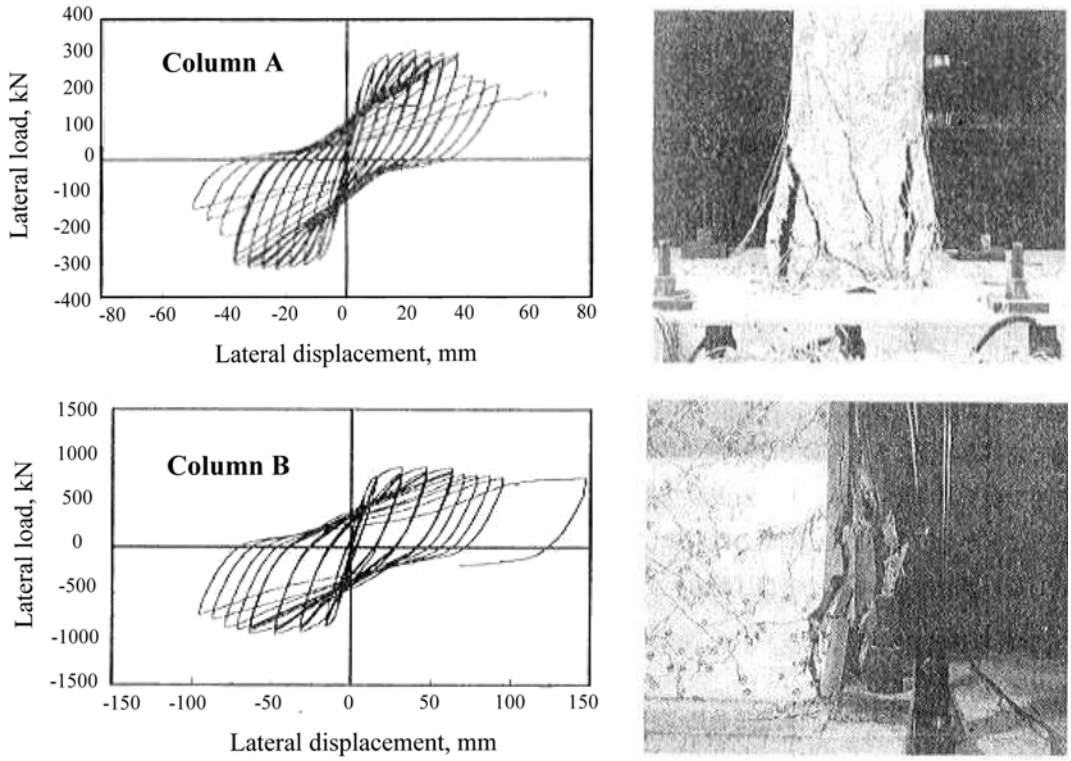

Fig. 13 Load-displacement curves and crack patterns observed in experiments (Masuda *et al.* 1997)

fibers by volume, and these columns are subjected to reversed cyclic lateral displacement under a constant axial compressive stress of 1 MPa.

The experimental results and observed crack pattern of these two columns are illustrated in Fig. 13. As can be seen in the figures, significant deterioration at the base occurred in column A. Although splitting cracks formed, the steel fibers bridged these cracks and maintained the integrity. Hence, the cover concrete did not detach completely and reinforcement buckling was not noticed. In column A, diagonal shear cracks appeared and these cracks widened during the later part of the loading, indicating that the column must have gone through significant inelastic shear deformation in the later phase. It might be the cause of the reduction in lateral load in the post-peak region and also the pinching mechanism observed in the load-displacement curve. In column B, the diagonal cracks did not widen, signifying that the associated shear deformation was elastic. Consequently, the pinching in the hysteresis loop is also not severe and the post-peak envelope does not show any load degradation. In column B, splitting cracks did not form, and cover concrete spalling as well as reinforcement buckling did not occur.

Both of these columns are modeled with frame elements and fiber analyses are performed twice; once using the normal RC material models and again using the proposed SFRC material models. The analytical load-displacement results are presented in Fig. 14. As the tested columns had 1% fiber content, the use of the SFRC models derived from the tests of specimens with 1% fibers is justified. In both sets of analyses, columns A and B yield at about 4 mm and 8 mm, respectively. Looking at the experimental hysteresis curves, it can be said that these values are close to the

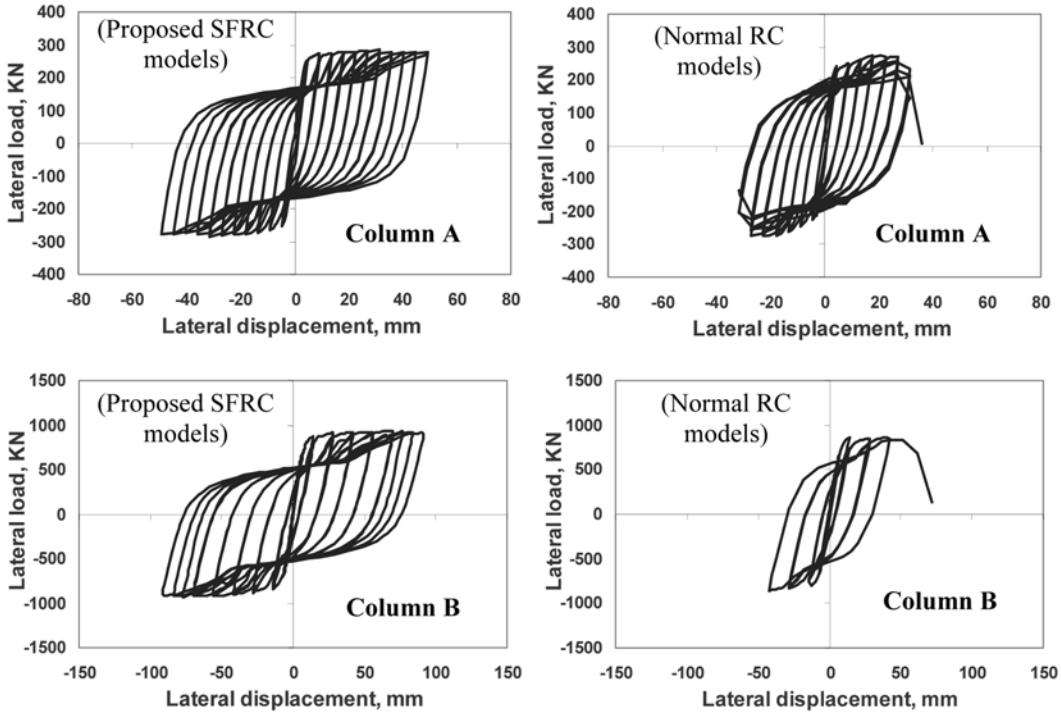

Fig. 14 Load-displacement relationships (analyses with normal RC & proposed SFRC models)

yielding displacements observed in the tests. The analyses with normal RC models predict that the columns A and B would collapse after the 30 mm and 50 mm displacement cycles respectively (i.e., ductility of 6~7), whereas in the tests these columns survived 50 mm and 100 mm displacement cycles respectively (i.e., ductility~12). In the analyses with normal RC models, spalling and buckling occur early in the post-peak range resulting in a premature failure. Obviously, the analytical load-displacement plots obtained by using the normal RC models are far from the corresponding experimental curves.

On the other hand, the analytical results obtained by using the proposed SFRC models show better agreement with the experimental results. The ability of both specimens to withstand the applied cyclic displacements is clearly reflected in the analytical results. More importantly, agreeing with the experimental observations, neither cover concrete did spall nor did the reinforcement buckling occur in the analysis. The maximum load, ability of the specimens to sustain higher ductility (more than 12) without collapse as well as the delay of spalling and buckling mechanisms could also be fairly predicted by the proposed SFRC models. Nevertheless, the analytical curves show less pinching than the experimental loops, mainly because the pinching is a prominent feature of inelastic cyclic shear response which is overlooked in the analyses. The restoring force starts reducing after 40 mm amplitude displacement cycles in column A test results, and this load degradation does not appear in the analytical result. The load degradation is attributed to the widening diagonal shear crack which is clearly visible (see Fig. 13), and the analysis was obviously not capable of capturing this. For more accurate prediction of the response of such shear-prone columns, cyclic shear behavior should be modeled and included in the constitutive relationship.

6. Conclusions

The EPF model and the tension softening/stiffening model, initially developed to represent compression and tension behaviors of normal concrete, are modified based on the results of standard SFRC cylinder compression tests and axial pullout tests of SFRC specimens. Thus obtained compression and tension envelopes of SFRC are combined with unloading and reloading loops typical of normal concrete to form a cyclic path-dependent uniaxial fiber model for SFRC. A model to predict the buckling length of main bars in SFRC members is also proposed. Thus determined buckling length and fracture energy of SFRC are used in an existing cover concrete spalling model to calculate the compressive strain corresponding to cover spalling in SFRC. To simulate cover concrete spalling, the compressive stress carried by the cover SFRC fibers is released once the spalling strain is reached. The proposed buckling length determination method also enables the effect of bar buckling in SFRC members to be included in an existing cyclic stress-strain relationship of main bars. Thus derived cyclic path-dependent material models of SFRC and reinforcing bars are encoded in a finite-element based fiber analysis tool which is used to perform cyclic analyses of SFRC columns.

The correlation between experimental and analytical results is found to improve drastically by using the proposed SFRC models instead of the normal RC models. In general, flexural response of SFRC columns could be predicted fairly by the proposed models. Agreeing with the actual behavior, the cover spalling and reinforcement buckling did not occur even in high deformation stage. The increase in ductility of SFRC columns compared to similar normal RC columns could also be predicted. Thus, a platform to enable analytical investigation of performance of SFRC structures is established through this research, but there are rooms for improvement. Modeling of cyclic shear behavior of SFRC and incorporating the generalized shear model in the frame analysis program needs to be done. The compression and tension envelopes of SFRC model are empirically derived based on the test results of SFRC with 1% fiber and the fiber content V_f is not explicitly used in the corresponding equations. The behavior of SFRC with different amount of fibers is expected to be different and these models need to be generalized for wider applicability.

References

An, X., Maekawa, K. and Okamura, H. (1997), "Numerical simulation of size effect in shear strength of RC beams", *J. Materials., Conc. Struct., Pavements,* JSCE, **564**(35), 297-316.

CEB (1996), *RC Elements under Cyclic Loading - State of the Art Report*, Thomas Telford.

Dhakal, R.P. and Maekawa, K. (2002a), "Modeling for postyield buckling of reinforcement", *J. Struct. Engrg.*, ASCE, **128**(9), 1139-1147.

Dhakal, R.P. and Maekawa, K. (2002b), "Path-dependent cyclic stress-strain relationship of reinforcing bar including buckling", *Engrg. Structs.*, **24**(11), 1383-1396.

Dhakal, R.P. and Maekawa, K. (2002c), "Reinforcement stability and fracture of cover concrete in reinforced concrete members", *J. Struct. Engrg.*, ASCE, **128**(10), 1253-1262.

Fanella, D. and Naaman, A.E. (1982), "Stress-strain properties of fiber reinforced mortar in compression", *ACI J.*, **82**(4), 475-583.

Hsu, L.S. and Hsu, C.T. (1994), "Stress-strain behavior of steel fiber high strength concrete under compression", *ACI Struct. J.*, **94**(4), 448-457.

Kosaka, Y., Tanigawa, Y. and Hatanaka, H. (1984), "Experimental study on inelastic stress-strain behavior of steel fiber reinforced concrete under compression", *Transactions of AIJ*, **337**, 15-24.

Maekawa, K. and Okamura, H. (1983), "The deformational behavior and constitutive equation of concrete using the elasto-plastic and fracture model", *J. of Faculty of Engrg., Univ. of Tokyo (B)*, **37**(2), 253-328.
Maekawa K. (2000), *General Information of COM3 (Concrete Model in 3-D) Version 9.5 – A User's Manual*. Dept. of Civ. Engrg., Univ. of Tokyo.
Masuda, A., Matsuoka, S., Matsuo, S. and Takeda, Y. (1997), "Static alternating cyclic loading tests of steel fiber reinforced concrete columns", *Proc. of JCI Annual Conf.*, **19**(2), 1521-1526, (in Japanese)
Matsuoka, S., Matsuo, S., Masuda, A. and Yanagi, H. (1997), "A test method for tensile property of steel-fiber-reinforced concrete", *J. Materials., Conc. Struct., Pavements,* JSCE, **564**(35), 145-153.
Menegotto, M. and Pinto, P.E. (1973), "Method of analysis of cyclically loaded RC plane frames including changes in geometry and non-elastic behavior of elements under normal force and bending", Preliminary Report, IABSE, **13**, 15-22.
Okamura, H. and Maekawa, K. (1991), *Nonlinear Analysis and Constitutive Models of Reinforced Concrete*, Gihodo Publication, Tokyo.
Someh, A.K. and Saeki, N. (1996), "Prediction for the stress-strain curve of steel fiber reinforced concrete", *Proc. of JCI Annual Conf.*, **18**(1), 1149-1154.